Control Co-design of Linear and Nonlinear Wave Energy Converters

Habeebullah Abdulkadir
Department of Aerospace Engineering,
Iowa State University,
Ames, IA 50010, USA.

Ossama Abdelkhalik
Department of Aerospace Engineering
Iowa State University,
Ames, IA 50010, USA.

***Abstract*—This work presents the control co-design of a linear cylindrical and a spherical single-body wave energy converter (WEC). By control co-design, the goal is to concurrently design an energy-maximizing controller with the device. The nonlinear Froude-Krylov (FK) forces resulting from the changing cross-sectional area of the floater at the water surface are leveraged to improve the performance of the spherical device. Linear and nonlinear damping control formulations were presented with their coefficients as optimization variables. This work does not seek to compare the performance of the linear and nonlinear devices; rather, it presents a formulation for the control co-design of these systems.**

***Index Terms*—Wave energy converter, Control co-design, Optimal control, Nonlinear model, Nonlinear Froude-Krylov forces.**

I. Introduction

Wave energy converters design and control have been researched thoroughly over the past few decades in an effort to achieve the potential of decarbonizing energy sources. The point absorber [1] WEC design is one of the popular designs. These devices are characterized by dimensions smaller than the wavelength of incoming waves. Unlike other mechanical systems, these devices seek to resonate with the exciting wave frequency for maximum energy absorption. Control methods [2–9] have been developed to modify the dynamic of the device for this purpose.

Most mathematical models of these devices are often linear models. However, a more accurate model will include the nonlinearities affecting the device and could lead to an even further increase in energy extracted. WEC nonlinearities can come from different sources, including but not limited to geometric, mooring, power take-off (PTO), hydrodynamic nonlinearity, and many more. Researchers in [10–18] have developed control formulations to leverage several nonlinearities.

Control design often comes after the device has been designed; however, for many systems, it has been observed that device design and control design are more coupled, and there is a need for a control co-design approach. Therefore, in this work, we formulate and develop an approach to concurrently optimize the WEC and the control. This formulation is presented for a linear cylindrical WEC and nonlinear spherical WEC device.

For a linear device like the cylinder, the hydrostatic and dynamic forces are calculated over a constant wetted area; however, for a sphere with a varying geometry at the water surface, the pressure needs to be integrated over the submerged surface instantaneously. An efficient closed-form algebraic formulation for approximating nonlinear Froude-Krylov (FK) forces developed in [19, 20] is adopted. The paper is organized as follows. Section II establishes a linear dynamic model for a simplified WEC device. The algebraic nonlinear FK force formulation is presented in section III. Section IV shows the nonlinear dynamics. The control formulations were discussed in Section V. Simulation results are presented in Section VI. And finally, we conclude in Section VII.

II. Linear System dynamics for cylindrical WEC

A simple WEC model can be represented as a second order mass-spring-damper system, as shown in Fig. 1.

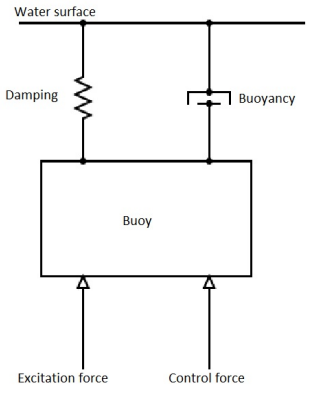

Fig. 1. Schematic of a simplified WEC device

Assuming small wave height and small motion amplitude, the motion of a floater restricted to heave motion only can be modeled using a 1-DoF (heave only) linear equation of motion as [21]:

$$m\ddot{z}(t) = \overbrace{\int_{-\infty}^{\infty} h_f(\tau)\eta(t-\tau,z)d\tau}^{\text{excitation force, } f_e} + f_s \quad (1)$$

$$\overbrace{-m_\infty \ddot{z}(t) - \int_{-\infty}^{t} h_r(\tau)\dot{z}(t-\tau)d\tau}^{\text{radiation force } f_r} - u \quad (2)$$

where z is the heave displacement of the buoy from the sea surface, t is the time, m is the buoy mass, u is the control force, and $f_s = -Kz$ is the hydrosatic restoring force. f_e is the excitation force, where η is the wave surface elevation at buoy centroid and h_f is the impulse response function defining the excitation force in heave. f_r is the radiation force, where m_∞ is a frequency-dependent added mass, and h_r is the impulse response function defining the radiation force in heave. The dynamics of the motion of the floater can be written as [22]:

$$m\ddot{x} = f_e + f_r + f_s + u \quad (3)$$

III. Algebraic nonlinear Froude-Krylov force modeling

This formulation is based on the development of algebraic calculation of the nonlinear FK forces applicable to axisymmetric heaving point absorbers by [19]. For a spherical device like Fig. 2, the total Froude-Krylov (FK) force is the hydrostatic force FK_{st} and the dynamic force FK_{dy}. The nonlinear hydrostatic force is the difference between the gravity force F_g and the static FK force on the buoy.

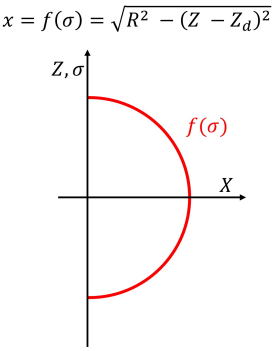

Fig. 2. Schematic of a simplified WEC device

$$F_{FK} = F_g - \int_0^{2\pi}\int_{\sigma_1}^{\sigma_2} P(t)\boldsymbol{n}dS \quad (4)$$

$P(t)$ is the instantaneous pressure, on the infinitesimal element $\boldsymbol{n}dS$. The total pressure for deep water waves using Airy's wave theory is defined as:

$$P(t) = \rho g e^{\chi\sigma}\eta(t)cos(\omega t) - \rho g\sigma(t) \quad (5)$$

where ρ is the water density, g is the gravitational acceleration, $\eta(t)$ is the free surface elevation, χ is the wave number, $\sigma(t)$ is the positive upwards height of the device and ω is the wave frequency. The magnitude of the heaving Froude-Krylov forces becomes:

$$F_{FK} = \int_0^{2\pi}\int_{\sigma_1}^{\sigma_2} P(t)f'(\sigma)f(\sigma)d\sigma d\theta \quad (6)$$

$$F_{FK} = \int_0^{2\pi}\int_{\sigma_1}^{\sigma_2} (\rho g e^{\chi\sigma}\eta(t)cos(\omega t) - \rho g\sigma(t))f'(\sigma)f(\sigma)d\sigma d\theta \quad (7)$$

At the equilibrium position, h_0 is the draft of the buoy, $Z_d(t)$ is the instantaneous displacement of the buoy from its equilibrium position. The algebraic FK forces for the spherical and sloped line profiles described in Fig. 2 can be computed using the equations defined in Eq. (7). The limit of integration based on the free surface elevation and the draft of the buoy can be described as:

$$\sigma_1 = -h_0 + Z_d(t) - \eta(t),\ \sigma_2 = 0 \quad (8)$$

For example, the nonlinear hydrostatic and hydrodynamic forces of a spherical buoy can be computed as:

$$F_{FK_{static}} = F_g - 2\pi\rho g\left[\frac{(-R+Z_d-\eta(t))^3}{3} - \frac{(-R+Z_d-\eta(t))^2}{2}(Z_d+\eta(t))\right] \quad (9)$$

$$F_{FK_{dynamic}} = -\frac{2\pi\rho g\eta(t)}{\chi}cos(\omega t)\left[\left(\sigma - Z_d + \eta(t) - \frac{1}{\chi}\right)e^{\chi\sigma}\right]_{\sigma_1}^{\sigma_2} \quad (10)$$

Similarly, the algebraic form of the static and dynamic FK forces can be computed for sloped lines or other shapes that can be represented with algebraic equations. [19] validated this method of computing FK forces against a more computationally expensive remeshig method and only had about a 2% error.

IV. NonLinear dynamics for spherical WEC

When the small wave height and motion assumption does not hold, the motion of the floater is restricted to heave motion only, and the nonlinear equation of motion for a 1-DoF (heave only) solo WEC can be written as:

$$m\ddot{z}(t) = F_{NLFK} - u - \mu\ddot{z}(t) - c\dot{z} \quad (11)$$

$$F_{NLFK} = F_{FK_{dyn}+F_{FK_{st}}} \quad (12)$$

where z is the heave displacement of the buoy from the sea surface, t is the time, m is the buoy mass, u is the control force, and $F_{FK_{st}}$ is the static FK force and $F_{FK_{dyn}}$ is the dynamic FK force. In the case of a regular wave environment, the radiation force reduced to a linear damping and an added mass term.

V. Control co-design formulation

In this section, the two optimization problems are presented. The first is the control size optimization of a linear cylindrical device, and the second is the optimal co-design of a nonlinear spherical WEC having comparable volume to the linear cylinder.

A. Optimization of linear cylindrical device

In the current optimization problem, we want to determine the dimension of a cylindrical WEC (radius and draught) as in Fig. 3, which maximizes the power extracted from the waves. The optimization objective is formulated as follows:

$$J = \frac{1}{T}\int_0^{t_f}\{-u(t)x_2(t)\}dt$$

$$\begin{aligned} s.t.\ R \in\ & [R_{min.}\ R_{max.}] \\ D \in\ & [D_{min.}\ D_{max.}] \\ B_{pto} \in\ & [B_{pto-min.}\ B_{pto-max.}] \end{aligned} \tag{13}$$

A linear damping control formulation, $u = -B_{pto}\dot{z}$, was used in the optimization. Where R is the radius of the cylinder, D is its submerged draft and B_{pto} is the PTO damping coefficient. The best-performing R and D are returned as the best dimensions for the specified wave condition.

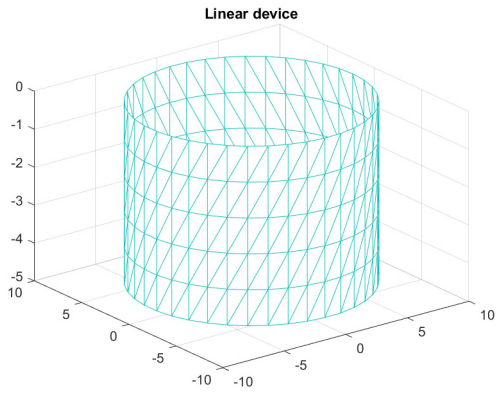

Fig. 3. Cylinder.

B. Control co-design for a nonlinear spherical device

In the current problem, the goal is to determine the size of the device and its nonlinear control formulation that maximizes the power extraction by the nonlinear device considered. The optimization objective is the power from the device:

$$J = \frac{1}{T}\int_0^{t_f}\{-u(t)x_2(t)\}dt$$

$$\begin{aligned} s.t.\ R \in\ & [R_{min.}\ R_{max.}] \\ \alpha \in\ & [\alpha_{min.}\ \alpha_{max.}], \\ \beta \in\ & [\beta_{min.}\ \beta_{max.}], \\ Volume_{sphere} \leq\ & Volume_{cylinder.} \end{aligned} \tag{14}$$

where R is the sphere's radius, the device's total volume is constrained to not exceed a reference volume, which is to be decided by the designer based on economic or technical reasons. Similar to the formulation proposed in [23], the nonlinear damping control is formulated as:

$$u = -\alpha B(\omega)\dot{z} - \beta B(\omega)\dot{z}^3 \tag{15}$$

where α and β are control coefficients to be optimized, $B(\omega)$ is the maximum hydrodynamic damping force on the device and $\dot{z}$ is the heave velocity of the device. The bounds of the variables are described in Table I. The optimization is completed using Genetic algorithm [24]. A flowchart of the optimization setup is presented in Fig. 4.

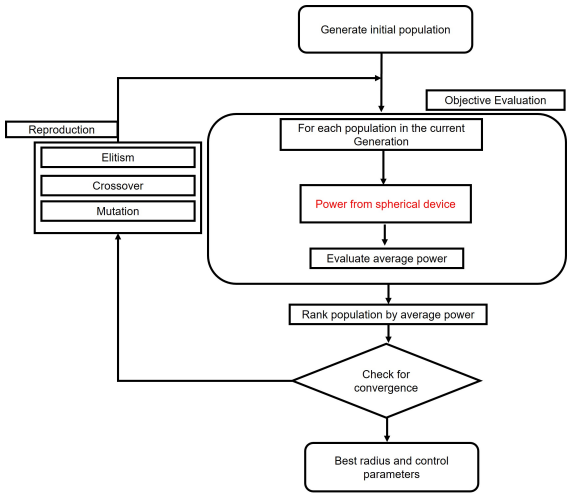

Fig. 4. GA flowchart for control co-design optimization.

TABLE I
CONSTRAINTS ON THE OPTIMIZATION PARAMETERS.

Parameter	Unit	Lower Bound	Upper Bound
R	m	2	15
α	-	0.001	5
β	-	0.001	5

VI. SIMULATION RESULTS

The devices optimized in this section are a linear cylindrical floater and a nonlinear spherical floater. The wetted surface of the devices is optimized for best hydrodynamic interaction; a site with a wave period $T = 6$ s and wave height $H = 0.8222$ m was considered. The hydrodynamic parameters are computed from the linear hydrodynamic solver NEMOH. The maximum control force availed by the PTO is $\Upsilon = 1e8$ N.

The optimum radius and draught of the cylindrical device were 8.23 m and 4.73 m [25], respectively. The linear damping coefficient was found as $B_{pto} = 2.3765e6N.s/m$. The Response Amplitude Operator (RAO) of the optimized device is plotted in Fig. 5. The wave frequency at the site is the vertical blue line. The device's maximum response of 1.95 m corresponds

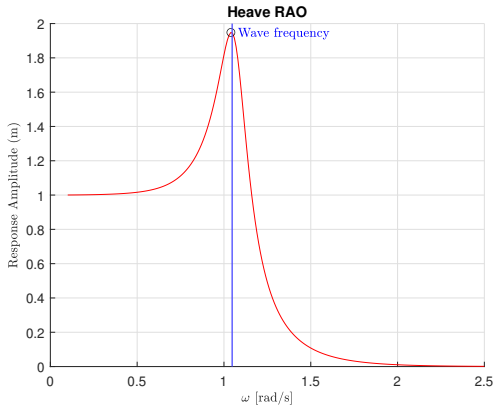

Fig. 5. RAO of an optimized isolated device.

to the wave frequency. The device's submerged volume is $V = 1.0065e03\ m^3$. The volume of this optimized cylinder is considered the maximum allowable volume for the nonlinear spherical device in Fig. 6.

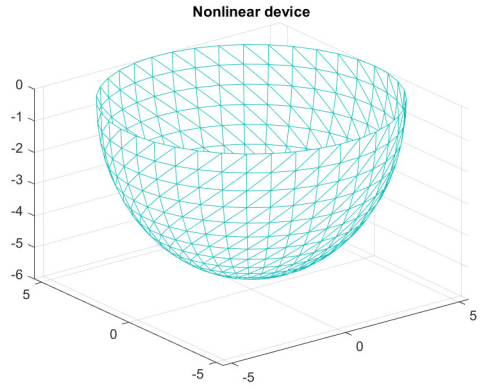

Fig. 6. Sphere.

In the nonlinear device control co-design problem, the control developed in Section V is optimized concurrently with the spherical device dimension in the same regular wave environment as the cylindrical device. A few results from a 40s optimization run for the nonlinear device (NLD) optimization is presented in Table II, where $B(\omega) = 1.1745e5$. The simulation of one of the solutions is plotted against the cylindrical linear device (LD).

Fig. 7 shows the exciting wave amplitude, and the resulting displacement and velocity of both the linear and nonlinear device are plotted in Fig. 8 and Fig. 9, respectively. The nonlinear motion of the spherical device can be observed from the plot, while the motion of the linear device is perfectly sinusoidal. In the steady state region, the devices have a similar magnitude of displacements; however, the velocity of the nonlinear device is significantly larger.

TABLE II
THE OPTIMIZED CONTROL PARAMETERS FOR A SPHERE

S/N	radius	α	β	Power (W)
1	7.3329	1.3130	0.5195	4.9605e06
2	7.5875	2.9779	2.6108	5.4014e06
3	7.7500	0.7902	2.1668	5.8996e06
4	6.1548	1.8679	2.3761	2.8313e06
5	5.4273	2.8889	1.7983	1.9030e06
6	7.8328	0.6683	2.9577	6.0751e06
7	7.1092	1.0851	1.8924	4.2166e06
8	7.3988	2.6808	2.4658	4.9802e06
9	7.4849	2.9995	0.3518	4.9057e06
10	7.8123	2.1212	2.7373	5.8321e06

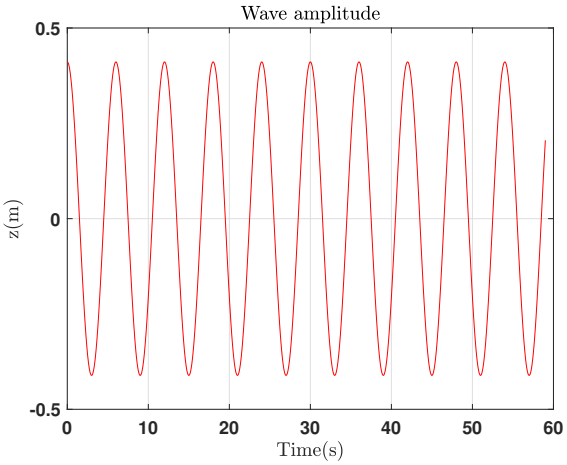

Fig. 7. Exciting wave amplitude.

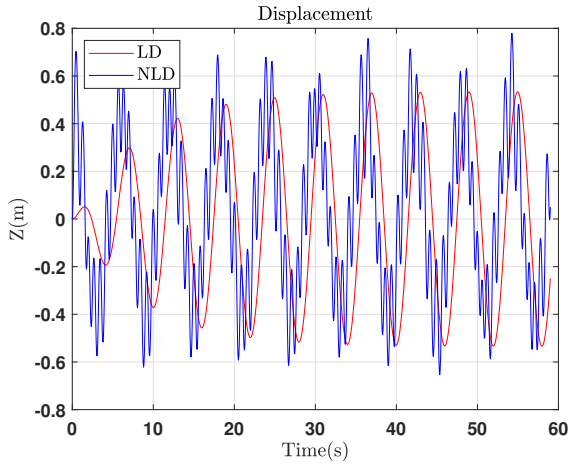

Fig. 8. Displacements.

The excitation force (F_e) on the linear device and the dynamic nonlinear FK force acting on the spherical device are plotted in Fig. 10. The magnitude of NLFK force acting on the spherical device is larger and not as sinusoidal as the linear excitation force. It can be observed that the NLFK force goes to zero at intervals, this is when the motion of the device grows to be too large that the device goes out of the water or sinks. The

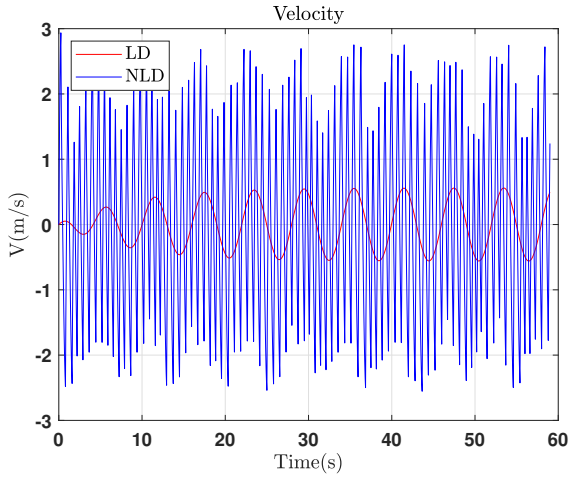

Fig. 9. Velocity.

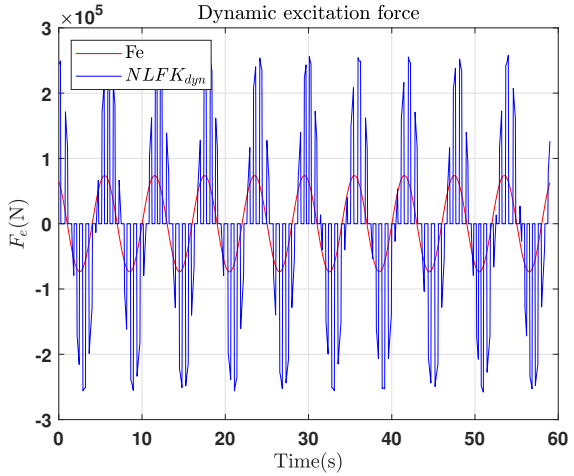

Fig. 10. Dynamic FK forces.

linear and nonlinear PTO force is presented in Fig. 11. The magnitude of forces generated by the NLD control is significantly larger than that from the LD control.

The power from both devices is subplotted in Fig. 12. The average power for the linear device over the period of simulation is $3.3435e4W$, which the average power output to the nonlinear device is $1.6392e6W$, which is a significantly higher power output by the NLD. A cumulative power plot is presented in Fig. 13. Although power comparison is not the goal of this work, the NLD consistently outperforms the LD in all simulations.

VII. Conclusion

A control co-design approach was presented for linear and nonlinear WEC design. The spherical wave energy converter leverages the nonlinear Froude-Krylov (FK) forces to maximize the power output. The FK forces were derived algebraically; the control structure was formulated for linear and nonlinear devices and optimized alongside the WEC device. Simulation results presented

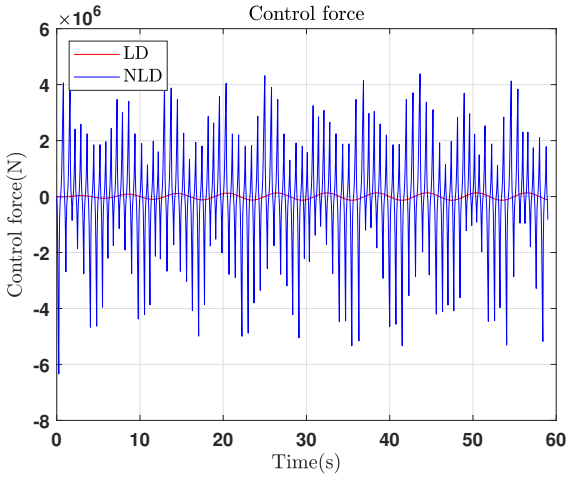

Fig. 11. PTO force.

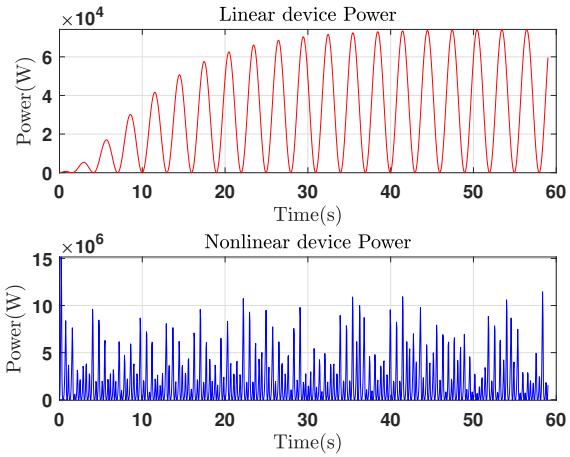

Fig. 12. Power.

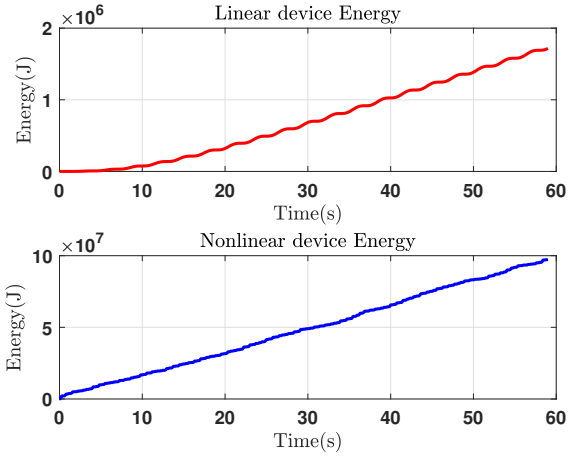

Fig. 13. Energy.

in this paper show that the overall performance of the nonlinear device (NLD) obtained from the co-design approach achieved significantly higher power output than

that of the linear device (LD). The wave considered in this current work is monochromatic. Future work will develop and test the performance of the control co-design approach for devices in irregular wave environments.

Acknowledgment

This paper is based upon work supported by NSF, Grant Number 2048413. The research reported in this paper is partially supported by the HPC@ISU equipment at Iowa State University, some of which has been purchased through funding provided by NSF under MRI grant number 1726447.

References

[1] J. Pastor and Y. Liu, "Frequency and time domain modeling and power output for a heaving point absorber wave energy converter," *International Journal of Energy and Environmental Engineering*, vol. 5, no. 2, pp. 1–13, 2014.

[2] N. Faedo, S. Olaya, and J. V. Ringwood, "Optimal control, mpc and mpc-like algorithms for wave energy systems: An overview," *IFAC Journal of Systems and Control*, vol. 1, pp. 37–56, 2017.

[3] H. Abdulkadir and O. Abdelkhalik, "Optimal constrained control of wave energy converter arrays," in *2022 American Control Conference (ACC)*, 2022, pp. 3100–3105.

[4] M. A. Shabara, S. Zou, and O. Abdelkhalik, "Numerical investigation of a variable-shape buoy wave energy converter," in *International Conference on Offshore Mechanics and Arctic Engineering*, vol. 85192. American Society of Mechanical Engineers, 2021, p. V009T09A013.

[5] J. Hals, J. Falnes, and T. Moan, "Constrained optimal control of a heaving buoy wave-energy converter," *Journal of Offshore Mechanics and Arctic Engineering*, vol. 133, no. 1, 2011.

[6] G. Li, G. Weiss, M. Mueller, S. Townley, and M. R. Belmont, "Wave energy converter control by wave prediction and dynamic programming," *Renewable Energy*, vol. 48, no. 0, pp. 392 – 403, 2012.

[7] S. Zou, O. Abdelkhalik, R. Robinett, G. Bacelli, and D. Wilson, "Optimal control of wave energy converters," *Renewable energy*, vol. 103, pp. 217–225, 2017.

[8] D. Wilson, G. Bacelli, R. G. Coe, D. L. Bull, O. Abdelkhalik, U. A. Korde, and R. D. Robinett III, "A comparison of wec control strategies," *Sandia National Laboratories Tech. Rep. SAND2016-4293*, vol. 10, p. 1431291, 2016.

[9] O. Abdelkhalik and H. Abdulkadir, "Optimal control of wave energy converters," in *OCEANS 2021: San Diego – Porto*, 2021, pp. 1–5.

[10] S. Zou, J. Song, and O. Abdelkhalik, "A sliding mode control for wave energy converters in presence of unknown noise and nonlinearities," *Renewable Energy*, vol. 202, pp. 432–441, 2023.

[11] G. Bacelli, R. Genest, and J. V. Ringwood, "Nonlinear control of flap-type wave energy converter with a non-ideal power take-off system," *Annual Reviews in Control*, vol. 40, pp. 116–126, 2015.

[12] G. Giorgi and J. V. Ringwood, "A compact 6-dof nonlinear wave energy device model for power assessment and control investigations," *IEEE Transactions on sustainable energy*, vol. 10, no. 1, pp. 119–126, 2018.

[13] J. Na, B. Wang, G. Li, S. Zhan, and W. He, "Nonlinear constrained optimal control of wave energy converters with adaptive dynamic programming," *IEEE Transactions on Industrial Electronics*, vol. 66, no. 10, pp. 7904–7915, 2018.

[14] D. G. Wilson, G. Bacelli, R. Robinett III, and O. Abdelkhalik, "Nonlinear control design for nonlinear wave energy converters." Sandia National Lab.(SNL-NM), Albuquerque, NM (United States), Tech. Rep., 2018.

[15] D. G. Wilson, R. D. Robinett III, G. Bacelli, O. Abdelkhalik, and R. G. Coe, "Extending complex conjugate control to nonlinear wave energy converters," *Journal of Marine Science and Engineering*, vol. 8, no. 2, p. 84, 2020.

[16] O. Abdelkhalik and S. Darani, "Optimization of nonlinear wave energy converters," *Ocean Engineering*, vol. 162, pp. 187–195, 2018.

[17] T. Demonte Gonzalez, G. G. Parker, E. Anderlini, and W. W. Weaver, "Sliding mode control of a nonlinear wave energy converter model," *Journal of Marine Science and Engineering*, vol. 9, no. 9, p. 951, 2021.

[18] M. Richter, M. E. Magana, O. Sawodny, and T. K. Brekken, "Nonlinear model predictive control of a point absorber wave energy converter," *IEEE Transactions on Sustainable Energy*, vol. 4, no. 1, pp. 118–126, 2012.

[19] G. Giorgi and J. V. Ringwood, "Computationally efficient nonlinear froude–krylov force calculations for heaving axisymmetric wave energy point absorbers," *Journal of Ocean Engineering and Marine Energy*, vol. 3, pp. 21–33, 2017.

[20] G. Giorgi, S. Sirigu, M. Bonfanti, G. Bracco, and G. Mattiazzo, "Fast nonlinear froude–krylov force calculation for prismatic floating platforms: a wave energy conversion application case," *Journal of Ocean Engineering and Marine Energy*, vol. 7, no. 4, pp. 439–457, 2021.

[21] W. Cummins, W. Iiuhl, and A. Uinm, "The impulse response function and ship motions," 1962.

[22] J. Falnes, *Ocean waves and oscillating systems: linear interactions including wave-energy extraction*. Cambridge university press, 2002.

[23] J. Song, O. Abdelkhalik, and S. Zou, "Genetic optimization of shape and control of non-linear wave energy converters," in *International Conference on Offshore Mechanics and Arctic Engineering*, vol. 84416. American Society of Mechanical Engineers, 2020, p. V009T09A036.

[24] D. Whitley, "A genetic algorithm tutorial," *Statistics and computing*, vol. 4, no. 2, pp. 65–85, 1994.

[25] H. Abdulkadir and O. Abdelkhalik, "Optimization of heterogeneous arrays of wave energy converters," *Ocean Engineering*, vol. 272, p. 113818, 2023.